Bistability and negative photoconductivity in optically induced real-space transfer

R. E. Kunz* and E. Schöll
Institute of Theoretical Physics, Technical University of Berlin, Hardenbergstrasse 36, D-1000 Berlin 12, Germany
(Received 13 August 1992)

Optically induced charge transport in a modulation-doped GaAs/$Al_xGa_{1-x}As$ heterostructure is studied theoretically. Intersubband excitation of electrons in the GaAs quantum well due to infrared absorption leads to their real-space transfer into the adjacent $Al_xGa_{1-x}As$ layer. We derive a system of nonlinear model equations considering as relevant physical mechanisms the generation-recombination processes in GaAs, longitudinal and transverse dielectric carrier relaxation, as well as resonant and nonresonant tunneling across the interface, and analyze its behavior with the methods of nonlinear dynamics. We predict optoelectronic bistability associated with different photoconductive responses between the two locally stable steady states corresponding to different types of tunneling prevalent: the regime of dominant resonant-tunneling currents shows negative differential photoconductivity, whereas the nonresonant tunneling state is practically invariant with respect to changes of the IR intensity.

I. INTRODUCTION

Nonlinear transport and instabilities associated with parallel charge transport in low-dimensional semiconductor structures have received much attention recently.[1,2] One important effect is the real-space transfer of electrons in modulation-doped GaAs/$Al_xGa_{1-x}As$ heterostructures. It can result from electron heating due to an applied electric field whereby the electrons are thermionically emitted from the high-mobility undoped GaAs well into the low-mobility n-$Al_xGa_{1-x}As$ barrier, thus producing negative differential conductivity, in analogy with the intervalley transfer in momentum space in the Gunn effect. In this paper we show that real-space transfer can also be induced by intersubband infrared excitation of carriers in the GaAs quantum well and subsequent tunneling into the adjacent $Al_xGa_{1-x}As$ layer, instead of field-induced carrier heating.

Electrically induced real-space transfer has been studied extensively both experimentally and theoretically.[1-5] ac-driven current oscillations[6] associated with negative differential conductivity were observed. A physical mechanism of a real-space transfer oscillator, which gives periodic[7] and chaotic[8,9] self-generated oscillations under dc conditions, has recently been proposed and numerically investigated. Also, using a reduced model, bistability and hysteretic switching transitions between oscillatory and stationary states were predicted.[10]

Although direct infrared absorption experiments between quantum well (QW) states in GaAs/$Al_xGa_{1-x}As$ heterostructures[11] and intersubband-induced photocurrents detected by applying a bias perpendicular to the layers[12] were reported a few years ago, static measurements of optically induced photoconductivity parallel to the layers were not reported until recently, with first results showing *negative* photoconductivity.[13] Recent interest has been focused on optical properties of electric-field tunable quantum well structures, such as optically induced charge accumulation, optoelectronic bistability, etc.[14]

In the present paper we propose and numerically investigate a mechanism for intersubband excitation-induced charge transport parallel to the layers of a modulation-doped GaAs/$Al_xGa_{1-x}As$ heterostructure. Our aim is to develop a dynamic theory of real-space transfer due to the optically induced transitions between the two two-dimensional (2D) subbands in the GaAs quantum well, and subsequent resonant and nonresonant tunneling into the $Al_xGa_{1-x}As$ barrier whose potential profile is calculated self-consistently by considering the space-charge dynamics. The model is analyzed using the tools of nonlinear dynamical systems.

The organization of the paper is as follows. After introducing the relevant physical mechanisms (Sec. II), the model equations are derived (Sec. III) and investigated (Sec. IV). The resulting negative photoconductivity and optoelectronic bistability are discussed in Sec. V. Finally, in Sec. VI, we summarize.

II. THE RELEVANT PHYSICAL MECHANISMS

A sample as schematically shown in Fig. 1 will be considered. It consists of GaAs quantum wells of width $2L_1$ embedded in thick $Al_xGa_{1-x}As$ barriers of width $2L_2=2(L_2^u+L_2^d)$, which are heavily n doped in the center (width $2L_2^d$). The sample possesses a prism geometry and is illuminated on the edge by polarized monochromatic infrared radiation.[13]

The band structure of a single GaAs/$Al_xGa_{1-x}As$ layer sequence is shown schematically in Fig. 2. Since all the sequences are considered to be dynamically equivalent, we assume periodic boundary conditions. Taking into account experimentally used layer widths,[13] the GaAs QW contains two parabolic two-dimensional subbands, $S_1^{(1)}$ and $S_1^{(2)}$, occupied by an electron density (dimension, $1/m^3$) of $n^{(1)}(x,t)$ and $n^{(2)}(x,t)$, respectively. Separation of conduction-band electrons, which reside in the GaAs channel at low bias U_0 and low intensity I of the infrared (IR) irradiation, from their parent donors leads to band bending in the $Al_xGa_{1-x}As$ layer due to

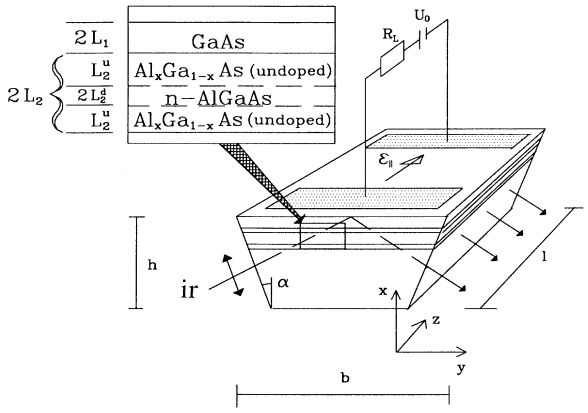

FIG. 1. Sample geometry (schematic): the sample is illuminated from the edge with IR radiation, which traverses the GaAs/$Al_xGa_{1-x}As$ layers twice, and is connected to an external circuit with bias voltage U_0 and load resistance R_L. The GaAs layers have a width of $2L_1$, the $Al_xGa_{1-x}As$ layers [width, $2L_2=2(L_2^d+L_2^u)$] are center doped in a region of width $2L_2^d$ and undoped outside.

the buildup of an internal electric field $\varepsilon_\perp$ perpendicular to the layers, which determines the interface potential barrier $\Phi_0 \equiv -e\int_0^{L_2}\varepsilon_\perp(x,t)dx$ and the potential loss in the doped region $\Phi_1 \equiv -e\int_{L_2^u}^{L_2}\varepsilon_\perp(x,t)dx$. Within the $Al_xGa_{1-x}As$ potential, only the energetically lowest two-dimensional subband S_2, assumed to be parabolic, is

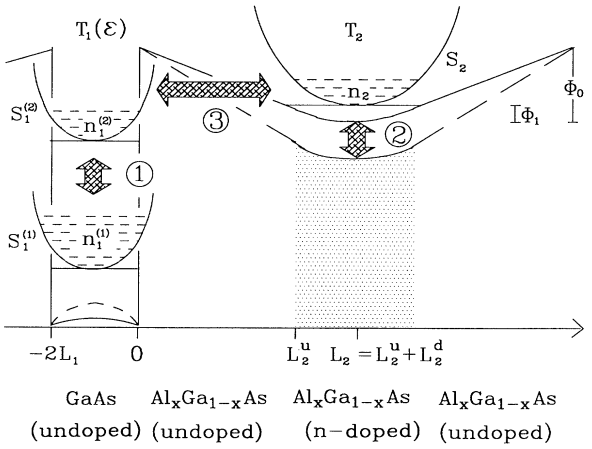

FIG. 2. Band structure of a GaAs/$Al_xGa_{1-x}As$ layer sequence (schematic), illustrating the system's relevant physical mechanisms: (1) the generation-recombination processes between the GaAs subbands $S_1^{(1)}$ and $S_1^{(2)}$ with averaged occupation densities $n_1^{(1)}$ and $n_1^{(2)}$, (2) the space-charge dynamics in the $Al_xGa_{1-x}As$ layer determining the total potential barrier Φ_0 and the potential loss in the doped region Φ_1, and (3) the tunneling currents which are responsible for the carrier exchange between the GaAs and $Al_xGa_{1-x}As$ region and thus determine the averaged carrier density in $Al_xGa_{1-x}As$, n_2. The electron temperature T_1 depends on the longitudinal electric field $\varepsilon_\parallel$. (The GaAs and $Al_xGa_{1-x}As$ layers are denoted by subscripts 1 and 2, respectively, while different subbands are denoted by superscripts.)

considered to have a nonvanishing occupation density $n(x,t)$, whose spatial average is denoted by $n_2 \equiv \int_0^{L_2} n(x,t)dx/L_2$.

The circled numbers in Fig. 2 correspond to the relevant physical mechanisms determining the system's dynamic behavior: (1) the generation-recombination kinetics between the two GaAs subbands, (2) the space-charge dynamics in the $Al_xGa_{1-x}As$ layer, and (3) the tunneling currents, which are responsible for the interaction between the two layers. Additionally we consider electron heating in the GaAs channel due to the applied bias U_0, resulting in an electron temperature T_1 there that depends on the longitudinal electric field $\varepsilon_\parallel$ parallel to the layers. Thermionic emission across the barrier Φ_0 can be neglected at the relatively small fields $\varepsilon_\parallel$ considered.

Based on the above physical mechanisms, we will derive a set of nonlinear differential equations for the spatially averaged carrier densities of the two GaAs subbands, $n_1^{(1)} \equiv \int_{-L_1}^0 n^{(1)}(x,t)dx/L_1$ and $n_1^{(2)} \equiv \int_{-L_1}^0 n^{(2)}(x,t)dx/L_1$, respectively, the dielectric relaxation of $\varepsilon_\parallel$, and the potential values Φ_0 and Φ_1 in the following section.

III. THE MODEL EQUATIONS

A. Generation-recombination kinetics

The temporal evolution of $n_1^{(1)}$ is governed by the rate equation

$$\begin{aligned}\dot{n}_1^{(1)} = (X+S)&\int_{-\infty}^{\infty}\mathcal{D}_1^{(2)}(E)f(E,E_{F_1}^{(2)},T_1)\\ &\times[1-f(E-\hbar\omega_{\hat{k}},E_{F_1}^{(1)},T_1)]dE\\ -X^*&\int_{-\infty}^{\infty}\mathcal{D}_1^{(1)}(E)f(E,E_{F_1}^{(1)},T_1)\\ &\times[1-f(E+\hbar\omega_{\hat{k}},E_{F_1}^{(2)},T_1)]dE\ . \end{aligned} \quad (1)$$

$\mathcal{D}_1^{(i)}(E) \equiv \Theta(E-E_1^{(i)})m_1^*/(\pi\hbar^2L_1)$ is the quasi-two-dimensional density of states corresponding to $S_1^{(i)}$, $i=1,2$, where m_1^* is the effective mass in GaAs, Θ is the Heaviside function, and $E_1^{(1)}$ and $E_1^{(2)}$ are the minimum energies of the ground and first excited subband, respectively, where the energetic origin is defined to be the value at the GaAs/$Al_xGa_{1-x}As$ interface. $\omega_{\hat{k}}$ is the frequency of the monochromatic infrared irradiation, whose photon energy $\hbar\omega_{\hat{k}}$ is assumed to be equal to $E_1^{(2)}-E_1^{(1)}$. $f(E,E_{F_1}^{(i)},T_1) \equiv \{1+\exp[(E-E_{F_1}^{(i)})/k_BT_1]\}^{-1}$, $i=1,2$, is the Fermi-Dirac distribution function with the Boltzmann constant k_B, quasi-Fermi energies $E_{F_1}^{(i)}$, $i=1,2$, and electron temperature T_1. The carriers in the GaAs channel can be considered thermalized at this temperature, since intrasubband relaxation takes place on a much smaller time scale than the relevant intersubband processes,[15] which are assumed to be photon absorption, stimulated emission of radiation, and intersubband relaxation with corresponding transition coefficients X^*, X, and S, respectively.

If one further assumes spatial homogeneity of the elec-

tron temperature inside the GaAs layer and small transversal currents across the barrier, the convective, diffusive, and electron-pressure-induced heat flow in the energy balance equation[16] can be neglected, and only the terms describing Joule's heating and the energy loss due to polar-optical scattering remain. If $j_\perp \varepsilon_\perp \ll j_\parallel \varepsilon_\parallel$ holds, where $j_\perp$ and $j_\parallel$ are the transversal and longitudinal current densities, respectively, and the constant energy relaxation time τ_e is introduced, we can then roughly estimate T_1 as a function of the applied electric field by

$$T_1 = T_L + \frac{e\mu_1\tau_e}{k_B}\varepsilon_\parallel^2 , \tag{2}$$

where μ_1 is the electron mobility in the GaAs channel.

X^* is calculated in the second quantization picture by using Fermi's golden rule[17] and considering the dipole-allowed transitions only. Assuming the direction of polarization to be perpendicular to the layers, which is a good approximation for small angle α (cf. Fig. 1), we obtain

$$X^* = \frac{e^2 n_r}{8\epsilon_1 \pi^2 \hbar c^3}\omega_{\hat{k}}^3 \left[\int_{-\infty}^{\infty} dx\, x\psi_1^{(1)}(x)\psi_1^{(2)}(x)\right]^2 N , \tag{3}$$

where n_r is the refractive index of GaAs, ϵ_1 is the permittivity of GaAs, and $\psi_1^{(i)}$, $i=1,2$ are the wave functions of the ground and first excited energy eigenstate of the GaAs potential, respectively. Neglecting space charges, they are given by the eigenfunctions of a square-well potential with finite height. N is the total photon number located within one GaAs layer. Applying the simple approximation that the intensity of the IR radiation is spatially constant within each GaAs layer, whereas it decreases exponentially during its double passage through all the layers, and taking into account the sample geometry, we obtain

$$N = 2\frac{L_1 b \ln n_r (T-1)}{\hbar\omega_{\hat{k}} c \sin\alpha \cos\alpha \ln T} I , \tag{4}$$

which allows us to express X^* in terms of the intensity of the incident radiation I if the optical transmission coefficient T is known.

X is equal to X^*.[17] Assuming the energy spacing $E_1^{(2)} - E_1^{(1)}$ between the GaAs subband minima to be bigger than the energy $\hbar\omega_{\mathrm{LO}}$ of LO phonons, polar optical scattering is the main intersubband relaxation mechanism.[15,18,19] In a phenomenological approach, we will thus assume S to be a constant given by experimental data.[18]

To deduce the final expression for $\dot{n}_1^{(1)}$, which is given by

$$\dot{n}_1^{(1)} = \frac{n_1^{(2)} - n_1^{(1)}}{e^{n_1^{(2)}/n_{c_1}} - e^{n_1^{(1)}/n_{c_1}}} \times \{[X(I)+S](e^{n_1^{(2)}/n_{c_1}} - 1) - X^*(I)(e^{n_1^{(1)}/n_{c_1}} - 1)\} , \tag{5}$$

the integrations in (1) were carried out, and the quasi-Fermi energies $E_{F_1}^{(i)}$ were substituted by the averaged occupation densities $n_1^{(i)}$, $i=1,2$ using

$$E_{F_1}^{(i)} = E_1^{(i)} + k_B T_1 \ln[\exp(n_1^{(i)}/n_{c_1}) - 1] , \tag{6}$$

where $n_{c_1} \equiv m_1^* k_B T_1/(\pi\hbar^2 L_1)$ is the quasi-two-dimensional degeneracy concentration in GaAs.

We emphasize that (5) and (6) are exact results which do not imply the approximation of nondegenerate Maxwell-Boltzmann statistics leading to the usual mass-action kinetics of generation-recombination processes. As a matter of fact, this approximation does not hold in the relevant experiments[13] which are conducted at helium temperature and with high effective doping concentrations, since the nondegeneracy condition $n_1^{(i)} \ll n_{c_1}$, $i=1,2$ is violated. The analytical evaluation of the integrals (1) is possible for 2D parabolic subbands, as opposed to the 1D or 3D case, due to the constant density of states.

$n_1^{(2)}$ as a function of time is governed by the equation of continuity

$$\dot{n}_1^{(2)} = -\dot{n}_1^{(1)} + \frac{1}{eL_1} j_\perp , \tag{7}$$

where $j_\perp \equiv (j_{1\to 2} - j_{2\to 1})$ holds, and $j_{1\to 2}$ and $j_{2\to 1}$ are the transversal electric currents through the GaAs/$Al_xGa_{1-x}As$ interface resulting from both resonant and nonresonant tunneling.

B. Space-charge dynamics

The calculation of the tunneling currents requires the knowledge of the ground-state energy of the transversal electron potential in the $Al_xGa_{1-x}As$ layer. The explicit potential form and its temporal behavior, however, is governed by the space-charge dynamics of the conduction-band electrons. In this section we will therefore find a description of the dielectric relaxation in the $Al_xGa_{1-x}As$ layer based on a small number of dynamic degrees of freedom, extending the technique used in Refs. 7, 9, and 10 for homogeneously doped layers to center doped ones.

The starting point is the Maxwell-Ampére law for the interior field $\varepsilon_\perp$, where the drift-diffusion approximation is used to describe the microscopic current density

$$\dot{\varepsilon}_\perp(x,t) = -\frac{e}{\epsilon_2}[\mu(x)n(x,t)\varepsilon_\perp(x,t) + D(x)n'(x,t)] + j_{\mathrm{ex}}(x,t)$$

$$\text{with } \mu(x) = \begin{cases} \mu_2^u, & 0 \le x < L_2^u \\ \mu_2^d, & L_2^u \le x < L_2 \end{cases} ,$$

$$D(x) = \begin{cases} D_2^u, & 0 \le x < L_2^u \\ D_2^d, & L_2^u \le x < L_2 \end{cases} . \tag{8}$$

The prime denotes the spatial derivative in the x direction, ϵ_2 is the permittivity in $Al_xGa_{1-x}As$, D_2^d and D_2^u are the diffusion coefficients in the doped and undoped $Al_xGa_{1-x}As$ regions, respectively, and j_{ex} is the external current density exchanged with the GaAs layer. Assum-

ing spatial homogeneity in longitudinal direction, the Maxwell equations show that j_{ex} cannot have a dependence on x. The periodic boundary conditions that we consider in this model then imply that j_{ex} vanishes for symmetry reasons.

$\varepsilon_\perp$ and the potential $\Phi(x,t)\equiv e\int_x^{L_2}\varepsilon_\perp(x',t)dx'$ hold and are assumed to meet the following boundary conditions:

$$\Phi(0)=-\Phi_0,\quad \Phi'(0)=-e\varepsilon_{\perp_0}\,,$$
$$\Phi(L_2^u)=-\Phi_1,\quad \lim_{x\nearrow L_2^u}\Phi'(x)=-e\varepsilon_\perp^-\,,$$
$$\lim_{x\searrow L_2^u}\Phi'(x)=-e\varepsilon_\perp^+\,, \tag{9}$$
$$\Phi(L_2)=0,\quad \Phi'(L_2)=0\,.$$

Poisson's equation is given by

$$\varepsilon_\perp'=\frac{e}{\epsilon_2}[N_D^*\Theta(x-L_2^u)-n(x)]\,, \tag{10}$$

where the doping density is approximated by a Heaviside function. $N_D^*\equiv N_D^+ + n_t$ is the effective doping density given by the concentration of ionized donors $N_D^+\equiv N_D - n_D$ (where N_D is the doping density and n_D is the electron density in the donors) and the concentration of ionized deep traps n_t, which results from persistent photoconductivity. Using (10) to substitute n in (8) leads after integration from 0 to L_2 and consideration of the boundary conditions to

$$\dot\Phi_0=\frac{e}{\epsilon_2}\left\{-\frac{\epsilon_2}{2}[\mu_2^u(\varepsilon_\perp^-)^2-\mu_2^d(\varepsilon_\perp^+)^2]+\frac{\epsilon_2}{2}\mu_2^u\varepsilon_{\perp_0}^2 +e(D_2^u\Delta n_2^u+D_2^d\Delta n_2^d)-N_D^*\mu_2^d\Phi_1\right\}, \tag{11}$$

where $\Delta n_2^u\equiv n(L_2^u)-n(0)$ and $\Delta n_2^d\equiv n(L_2)-n(L_2^u)$ result from the diffusion terms in (8). Analogously we obtain (12) by integrating (8) from 0 to L_2^u,

$$\dot\Phi_1=\frac{e}{\epsilon_2}\left\{\frac{\epsilon_2}{2}\mu_2^d(\varepsilon_\perp^+)^2+eD_2^d\Delta n_2^d-N_D^*\mu_2^d\Phi_1\right\}. \tag{12}$$

Integration of (10) from L_2^u to L_2 results in an expression for $\varepsilon_\perp^+$,

$$\varepsilon_\perp^+=-\frac{e}{\epsilon_2}L_2^d(N_D^*-n_2^d)\,, \tag{13}$$

where the averaged carrier density in the doped region $n_2^d\equiv\int_{L_2^u}^{L_2}n(x,t)dx/L_2^d$ has been introduced.

Analogously we obtain (14) by integrating (10) from 0 to L_2,

$$\varepsilon_{\perp_0}=\varepsilon_\perp^- -\varepsilon_\perp^+ +\frac{e}{\epsilon_2}[L_2^u n_2^u - L_2^d(N_D^*-n_2^d)]\,, \tag{14}$$

where $n_2^u\equiv\int_0^{L_2^u}n(x,t)dx/L_2^u$ is the averaged carrier density in the undoped region.

For a consistent description of the dielectric relaxation, the equation of continuity has to be met at the interface between the undoped and doped $Al_xGa_{1-x}As$ regions. Diffusion currents can be neglected within the mean free path of collisionless flight of the electrons. Beyond this finite length scale the average velocity of the carriers is much smaller due to the enhanced scattering of the electrons by phonons or by the barrier. This means that the assumption of constant electron density breaks down and transversal diffusion currents will become important. If we further assume that surface charges can be eliminated adiabatically,

$$\mu_2^u n^-\varepsilon_\perp^- = \mu_2^d n^+\varepsilon_\perp^+ \tag{15}$$

holds, where n^- and n^+ are the carrier concentrations on the undoped and doped side of the interface, respectively. We thus obtain

$$\varepsilon_\perp^- = \frac{\mu_2^d}{\mu_2^u}\frac{n_2^d}{n_2^u}\varepsilon_\perp^+\,, \tag{16}$$

since flat carrier density profiles in the doped and undoped regions can be assumed for thin doping widths (<100 Å), resulting in the relations $n^-\approx n_2^u$ and $n^+\approx n_2^d$. Using (16), insertion of Eqs. (13) and (14) in (11) and (12), respectively, then leads to the final formulas for the temporal evolution of Φ_0 and Φ_1,

$$\dot\Phi_0=\frac{e}{\epsilon_2}\left\{\frac{e^2}{2\epsilon_2}[L_2^d(N_D^*-n_2^d)]^2\left[\mu_2^d-\mu_2^u\left[\frac{\mu_2^d}{\mu_2^u}\frac{n_2^d}{n_2^u}\right]^2\right] +\mu_2^u\frac{e^2}{2\epsilon_2}\left[L_2^u n_2^u-\frac{\mu_2^d}{\mu_2^u}\frac{n_2^d}{n_2^u}L_2^d(N_D^*-n_2^d)\right]^2 -\mu_2^d N_D^*\Phi_1\right\}, \tag{17}$$

$$\dot\Phi_1=\frac{e\mu_2^d}{\epsilon_2}\left\{\frac{e^2}{2\epsilon_2}[L_2^d(N_D^*-n_2^d)]^2-N_D^*\Phi_1\right\}. \tag{18}$$

Thus, unlike the homogeneously doped case,[7,9,10] the barrier height Φ_0 and the averaged carrier concentration in the $Al_xGa_{1-x}As$ region n_2 does not suffice for a consistent description of the space-charge dynamics in the center doped case. The knowledge of Φ_1 and the averaged carrier density in both regions is necessary as well. Using carrier conservation given by $n_1L_1+n_2^uL_2^u+n_2^dL_2^d=N_D^*L_2^d$, where $n_1\equiv n_1^{(1)}+n_1^{(2)}$ was introduced for convenience, to substitute n_2^d, however, merely n_2^u must be expressed in terms of the other dynamic variables to guarantee a closed dynamic system.

To compute the ground-state energy E_2 of the $Al_xGa_{1-x}As$ potential, we simply assume it to be parabolic in the center region and linear elsewhere, which is a good approximation for small carrier concentrations in the undoped region and a flat carrier profile in the center. Knowledge of the boundary conditions (9) then allows the calculation of E_2 in second-order perturbation theory,

$$E_2=c_1(\Phi_1)\Phi_0+c_2(\Phi_1) \tag{19}$$

with

$$c_1 \equiv 2\sqrt{\gamma\pi}\left[\frac{1}{2\gamma L_2^u}e^{-\gamma(L_2^d)^2}-\frac{L_2^d}{L_2^u}\iota(\gamma)\right]-1$$

and

$$c_2 \equiv \frac{\hbar}{L_2^d}\left[\frac{\Phi_1}{2m_2^*}\right]^{1/2} + 2\sqrt{\gamma\pi}\Phi_1\left[\left[1+\frac{L_2^d}{L_2^u}-\frac{\gamma}{2(L_2^d)^2}\right]\iota(\gamma) - \frac{1}{2\gamma}e^{-\gamma(L_2^d)^2}\left[\frac{1}{L_2^u}-\frac{1}{L_2^d}\right]\right],$$

where $\gamma \equiv \sqrt{2m_2^*\Phi_1}/(\hbar L_2^d)$ was defined for convenience and $\iota \equiv \int_{L_2^d}^{\infty} e^{-\gamma x^2} dx$ has to be computed numerically.

C. Longitudinal dielectric relaxation

The longitudinal electric field $\varepsilon_\parallel$ is a time-dependent variable since the sample conductivity $\sigma = e(L_1\mu_1 n_1 + L_2^u\mu_2^u n_2^u + L_2^d\mu_2^d n_2^d)/(L_1+L_2)$ varies with the averaged carrier densities n_1, n_2^u, and n_2^d in the regions of different carrier mobilities μ_1, μ_2^u, and μ_2^d, respectively (where μ_1, $\mu_2^u \ll \mu_2^d$ hold due to enhanced impurity scattering in the doped $Al_xGa_{1-x}As$ region), thus influencing the voltage loss at the load resistance R_L and, due to the fixed bias voltage U_0, $\varepsilon_\parallel$ itself. Using Maxwell's and Kirchhoff's laws and assuming spatial homogeneity in the y and z directions, the dielectric relaxation of $\varepsilon_\parallel$ is given by

$$\dot{\varepsilon}_\parallel = \frac{1}{\epsilon_2\left[\frac{C}{C_i}+1\right]}[J_0-(\sigma_L+\sigma)\varepsilon_\parallel], \tag{20}$$

where $J_0 \equiv U_0/(R_L A)$ and $\sigma_L \equiv l/(R_L A)$ with the cross section $A \equiv (L_1+L_2)b$ of one $GaAs/Al_xGa_{1-x}As$ layer sequence were introduced for convenience. $C_i \equiv A\epsilon_2/l$ and C are the intrinsic sample capacity and the capacity of the external circuit, respectively, if $\epsilon_1 \approx \epsilon_2$ is assumed.

D. Resonant and nonresonant tunneling currents

When real-space transfer is induced by a strong electric field, the major coupling mechanism between the GaAs and $Al_xGa_{1-x}As$ layer is provided by thermionic emission, a process in which the hot electrons in the well spill over the energy barrier into the adjacent layer.[10] This mechanism can, however, be neglected in the case of low bias voltages ($U_0 \ll l[(|E_1^{(2)}|-k_BT_L)/(e\mu_1\tau_e)]^{1/2}$) and optical pumping, since the extended GaAs states generating a 3D band are practically vacant if low temperatures and thin GaAs layers are assumed.[20] Instead, carrier transport then takes place due to tunneling through the barrier. Depending on whether the energy levels of the electronic states localized on both sides of the barrier are lined up or not, resonant or nonresonant tunneling dominates.

Calculation of the current density of *resonant* tunneling j^{re} is performed under the assumption of the Schrödinger equation being separable in longitudinal and transversal components, of the conservation of longitudinal momentum in the tunneling process, and of the quasistationarity of the $Al_xGa_{1-x}As$ potential during tunneling. Then a coherent quantum-mechanical picture can be used, where the one-electron eigenfunctions of the two-layer system $\psi^{\pm} = (\psi_1^{(2)} \pm \psi_2)/\sqrt{2}$ are given in zero-order perturbation theory as the symmetric and antisymmetric superpositions of the localized wave functions $\psi_1^{(2)}$ and ψ_2, and the corresponding eigenvalues $E^{\pm}$ result from tunnel splitting of the eigenvalues $E_1^{(2)}$ and E_2 of the isolated systems. Examining the time dependence of the wave functions one finds that an originally localized state oscillates between the regions on both sides of the barrier with a frequency $\nu_{re} = \Delta E/(2\pi\hbar)$ where $\Delta E = E^+ - E^-$ is the energy splitting.[21,22] Thus, summing over all electrons and considering conservation of the longitudinal momentum, expressions for the electric current densities in the resonant case, denoted by (re), are obtained,

$$j_{1\to 2}^{(re)} = \frac{eL_2}{\pi\hbar}\Delta E n_2 , \quad j_{2\to 1}^{(re)} = \frac{eL_1}{\pi\hbar}\Delta E n_1^{(2)} . \tag{21}$$

Applying the method used in Ref. 23 to a system with different effective masses on each side of the barrier, the energy splitting can be computed under the assumption $E_1^{(2)} = E_2$,

$$\Delta E = \frac{\hbar^2}{2}\left[\frac{1}{m_1^*}+\frac{1}{m_2^*}\right]\left[\psi_{II}^{(if)}\frac{d}{dx}\psi_I^{(if)} - \psi_I^{(if)}\frac{d}{dx}\psi_{II}^{(if)}\right], \tag{22}$$

where $\psi_{I/II}^{(if)}$ and $d\psi_{I/II}^{(if)}/dx$ are the interface values of the relevant localized wave functions in the regions 1 and 2, respectively (normalized to regions 1 and 2, respectively) and their derivatives. $\psi_I^{(if)}$ and $d\psi_I^{(if)}/dx$ are obtained from $\psi_1^{(2)}$ and $d\psi_1^{(2)}/dx$ by renormalization. For the computation of $\psi_{II}^{(if)}$ and its derivative, we approximate the $Al_xGa_{1-x}As$ potential by a symmetric triangular potential, since we assume $L_2^u \gg L_2^d$. Neglecting renormalization, we then obtain

$$\psi_{II}^{(if)} = \mathrm{Ai}[\alpha_{Ai}^{2/3}L_2 - \xi_M^{(1)}] , \tag{23}$$

$$\frac{d}{dx}\psi_{II}^{(if)} = -\alpha_{Ai}^{2/3}\mathrm{Ai}'[\alpha_{Ai}^{2/3}L_2 - \xi_M^{(1)}] , \tag{24}$$

where $\alpha_{Ai} \equiv 2m_2^*(\Phi_0-\Phi_1)^2/[\hbar^2(L_2^u)^2]$ holds, and $\xi_M^{(1)}$ is the first maximum of the Airy function $\mathrm{Ai}(x)$, which has to be computed numerically.

Coherent resonant tunneling not only occurs when the eigenenergies of the localized states $E_1^{(2)}$ and E_2 exactly coincide. It is rather a resonant phenomenon leading to maximum tunneling currents in case of exact alignment, but also taking place for small deviations.[22] This will qualitatively be taken into account in our model by assuming the resonant-tunneling current to be proportional to the overlap η of the energetic "windows" $[(E_1^{(2)}-\Delta E)/2, (E_1^{(2)}+\Delta E)/2]$ and $[(E_2-\Delta E)/2, (E_2+\Delta E)/2]$, which are created by tunnel splitting of $E_1^{(2)}$ and E_2. Multiplying (21) by

$$\eta(E_2,\Delta E) = \begin{cases} \Delta E - |E_2 - E_1^{(2)}|, & \Delta E \geq |E_2 - E_1^{(2)}| \\ 0 \quad \text{otherwise} , \end{cases} \tag{25}$$

after subtraction and use of carrier conservation we then obtain

$$j^{(\mathrm{re})}=\frac{e}{\pi\hbar}\eta(\Phi_0,\Phi_1)[N_D^* L_2^d-(n_1^{(1)}+2n_1^{(2)})L_1]\ , \tag{26}$$

which meets the above requirements. η is a dynamic variable due to the dependence of ΔE and E_2 on Φ_0 and Φ_1. Equation (22) is also considered to hold for $E_1^{(2)}\approx E_2$ and $E_1^{(2)}\neq E_2$.

Nonresonant tunneling, which describes incoherent total-energy-conserving traversing of a potential barrier due to the quantum-mechanical tunnel effect is basically possible for all values of E_2. It dominates when resonant tunneling vanishes due to a strong deviation of $E_1^{(2)}$ and E_2.

Assuming the participating subbands $S_1^{(2)}$ and S_2 to be thermalized with the electron temperatures T_1 and $T_2\equiv T_L$ ($T_2\equiv T_L$ results from the low mobility in the doped $Al_xGa_{1-x}As$ region) and quasi-Fermi energies $E_{F_1}\equiv E_{F_1}^{(2)}$ and E_{F_2}, respectively, their energy distribution can be described by the Fermi-Dirac function $f(E,E_{F_i},T_i)$, $i=1,2$, and the semiclassical ansatz (27) can be made for the current densities for nonresonant tunneling from region i to j, $j_{i\to j}^{(\mathrm{nr})}$, $i,j=1,2$, $i\neq j$:

$$j_{i\to j}^{(\mathrm{nr})}=eL_i\int_{-\infty}^{0}\mathcal{D}_j(E)f(E,E_{F_j},T_j)\Theta(E-E_i)\times[1-f(E,E_{F_i},T_i)]\tau(E)\nu_j(E_j)dE\ , \tag{27}$$

where $\mathcal{D}_i\equiv\Theta(E-E_i)m_i^*/(\pi\hbar^2L_i)$ for $i=1,2$, and $E_1\equiv E_1^{(2)}$ are the densities of states for subbands $S_1^{(2)}$ and S_2, respectively. $\nu_1\equiv(\Delta E_c+E_1^{(2)})/2\pi\hbar$ and $\nu_2\equiv(\Phi_0+E_2)/2\pi\hbar$ are the frequencies of hitting the barrier in regions 1 and 2, respectively, where a simple approximation similar to the treatment in α decay has been used.[24] $\tau(E)=\exp[-\Lambda(-E)^{3/2}]$ with $\Lambda\equiv 4\sqrt{2m_2^*}L_2^u/[(\Phi_0-\Phi_1)3\hbar]$ is the tunneling probability obtained from a WKB approximation.

Due to the $\exp[(-E)^{3/2}]$ term, the integral in (27) is not analytically solvable. Its approximation by the zero-temperature limit, where $f(E,E_{F_j},T_j)$ is substituted by $\Theta(E-E_{F_j})$, $j=1,2$, is not reasonable, since it would not exclude the unphysical case of decoupled GaAs and $Al_xGa_{1-x}As$ subsystems resulting from vanishing tunneling currents. Instead, we apply the mean value theorem, leading to

$$j_{i\to j}^{(\mathrm{nr})}=\frac{em_j^*}{\pi\hbar^2}\nu_j\exp[-\Lambda(-\xi^*)^{3/2}]\times\int_{\max(E_1^{(2)},E_2)}^{0}f(E,E_{F_j},T_j)\times[1-f(E,E_{F_i},T_i)]dE\ , \tag{28}$$

and approximate the mean value $\xi^*\in[\max(E_1^{(2)},E_2),0]$ by $\xi\equiv\sum_{i=1}^{2}\max(E_1^{(2)},E_2,E_{F_i})/2$. This approximation is good if the relative deviation of the quasi-Fermi energies E_{F_1} and E_{F_2} is small, which is the case for physically reasonable parameters as the numerical simulations show. The integral in (28) can then be calculated analytically if $T_1\approx T_2\equiv T_L$ is assumed. After expressing E_{F_1} and E_{F_2} by $n_1^{(2)}$ and n_2, respectively, using formulas corresponding to (6), we obtain $j^{(\mathrm{nr})}\equiv j_{1\to 2}^{(\mathrm{nr})}-j_{2\to 1}^{(\mathrm{nr})}$,

$$j^{(\mathrm{nr})}=\frac{ek_BT_L}{2\pi\hbar^3}\ln\left[\frac{\varphi_1+1}{\varphi_2+1}\right](\varphi_1-\varphi_2)^{-1}\times[m_2^*(\Phi_0+E_2)\varphi_2-m_1^*(\Delta E_c+E_1)\varphi_1]\times\exp[-\Lambda(-\xi)^{3/2}]\ , \tag{29}$$

where $\varphi_1\equiv\exp[-\beta\Theta(\delta E)\delta E][\exp(n_1^{(2)}/n_{c_1})-1]$ and $\varphi_2\equiv\exp[\beta\Theta(-\delta E)\delta E][\exp(n_2/n_{c_2})-1]$ with $\beta\equiv(k_BT_L)^{-1}$, $n_{c2}\equiv m_2^*k_BT_L/(\pi\hbar^2L_2)$, and $\delta E\equiv E_2-E_1^{(2)}$ were introduced for convenience. The total current density $j=j^{(\mathrm{re})}+j^{(\mathrm{nr})}$ is then given by Eqs. (26) and (29).

For the calculation of $n_2^u=n_2^{u(\mathrm{re})}+n_2^{u(\mathrm{nr})}$ we assume that all carriers in the undoped region stem either from resonant or nonresonant tunneling currents, where the contributions are denoted by $n_2^{u(\mathrm{re})}$ and $n_2^{u(\mathrm{nr})}$, respectively. Other factors influencing n_2^u such as diffusion will be neglected. Thus n_2^u can be expressed in terms of the tunneling current densities.

Within the framework of the coherent picture applied in this model, the time needed to traverse the potential barrier in resonant tunneling is given by $\tau_{\mathrm{re}}=\pi\hbar/\Delta E$ for all carriers alike. If $\Phi_0+E_2\approx\Phi_1$ holds, the undoped region coincides with the traversed potential barrier and we thus obtain

$$n_2^{u(\mathrm{re})}=\frac{\tau_{\mathrm{re}}}{eL_2^u}(j_{1\to 2}^{(\mathrm{re})}+j_{2\to 1}^{(\mathrm{re})})\ . \tag{30}$$

In the case of $n_2^{u(\mathrm{nr})}$, we neglect the dependence of the tunneling time and the width of the traversed barrier upon the total carrier energy, assuming the carriers with the least possible total energy $E=\max(E_1^{(2)},E_2)$ to determine the tunneling time τ_{nr} as well as the undoped region to coincide with the transversal barrier. Then $\tau_{\mathrm{nr}}=[-2m_2^*\max(E_1^{(2)},E_2)]^{1/2}L_2^u/(\Phi_0-\Phi_1)$ is obtained using a simple formula given in Ref. 25. Hence $n_2^{u(\mathrm{nr})}$ results as

$$n_2^{u(\mathrm{nr})}=\frac{\sqrt{2m_2^*}}{e}\frac{[-\max(E_1^{(2)},E_2)]^{1/2}}{\Phi_0-\Phi_1}(j_{1\to 2}^{(\mathrm{nr})}+j_{2\to 1}^{(\mathrm{nr})})\ , \tag{31}$$

where $j_{1\to 2}^{(\mathrm{nr})}+j_{2\to 1}^{(\mathrm{nr})}$ is given in (29), substituting the difference by a sum.

Equations (5), (7), (20), (17), and (18) represent our basic model. They constitute an autonomous nonlinear set of differential equations

$$\dot{\mathbf{x}}=\mathbf{F}(\mathbf{x}) \tag{32}$$

with $\mathbf{x}\equiv(n_1^{(1)},n_1^{(2)},\varepsilon_{\|},\Phi_0,\Phi_1)^T$, whose static and dynamic behavior will be analyzed in the following section.

IV. FIXED POINTS AND STABILITY ANALYSIS

The above system has one fixed point, being defined by vanishing temporal derivatives and denoted by an asterisk, in the dark regime ($I=0$), which splits up into three with incident IR intensities ($I>0$). These can be classified according to the type of tunneling current prevalent: the pair of resonant fixed points $\mathbf{x}^{*(r1)}$ and $\mathbf{x}^{*(r2)}$ describe a steady state, in which $j^{(re)} \gg j^{(nr)}$ and $n_2^{u(re)} \gg n_2^{u(nr)}$ hold, whereas in the nonresonant steady state $\mathbf{x}^{*(nr)}$ $j^{(re)}$ and $n_2^{u(re)}$ vanish.

The formation of $\mathbf{x}^{*(r1)}$ and $\mathbf{x}^{*(r2)}$, which only differ considerably in their Φ_0 component, is a direct implication of $j^{(re)}$'s resonance feature, which can easily be seen under the assumption of $j^{(nr)}=n_2^{u(nr)}=0$: Eqs. (5) and (7) lead to a third-order polynomial for $\exp[n_1^{(2)*}/n_{c_1}(\varepsilon_\parallel)]$ in the steady state, which yields a unique solution due to Descartes's sign rule. Thus $n_1^{(2)*}(\varepsilon_\parallel)$ and, using (5), $n_1^{(1)*}(\varepsilon_\parallel)$ can be computed. Subtracting (18) from (17) leads to a unique expression for $n_2^{u*}[n_1^{(1)*}(\varepsilon_\parallel), n_1^{(2)*}(\varepsilon_\parallel)]$. By inserting the functional form of $n_1^{(1)}$, $n_1^{(2)}$, and n_2^u in σ, one obtains the stationary current density versus electric-field characteristic $j_\parallel^*(\varepsilon_\parallel)\equiv\sigma(\varepsilon_\parallel)\varepsilon_\parallel$ (Fig. 3, Table I). For $I=0$ and $I=\infty$ it ascends linearly with a bigger slope in the first case whereas for $0<I<\infty$ it shifts from the $I=\infty$ line to the $I=0$ one with increasing $\varepsilon_\parallel$ and is therefore nonlinear. This corresponds to a transition from the low conductivity state (dotted line) to a high conductivity state (solid line) with increasing $\varepsilon_\parallel$, which becomes more pronounced and sets in later at larger I. The reason for this is that optically induced real-space transfer allows the electrons to stay in the low conductivity $Al_xGa_{1-x}As$ layer up to larger fields.

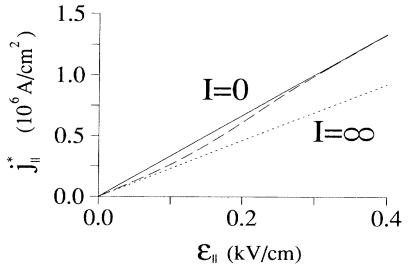

FIG. 3. Calculated stationary current density vs electric-field characteristics for different IR intensities I (numerical parameters cf. Table I). Whereas in the dark ($I=0$) the system is monostable with a linear characteristic (solid line), incident IR radiation leads to the formation of two locally stable branches corresponding to the respective tunneling currents prevalent: a nonresonant state (solid line), which is practically independent of I, and a resonant-tunneling state (dashed for $I=1$ W/cm^2, dotted for $I=\infty$), which changes with I.

Since the differential conductivity is therefore always positive, a unique stationary field $\varepsilon_\parallel^*$ given by the intersection of the device characteristic with the load line exists for each I, U_0, and R_L. Thus $n_1^{(1)*}$, $n_1^{(2)*}$, n_2^{u*}, and, using (12), Φ_1^* are determined uniquely. To find Φ_0 the so

TABLE I. Numerical parameters used in the simulations.

ΔE_c	248.5 meV	$\Delta E_c/E_G=0.85\pm0.03$ from Ref. 27. $E_G^{GaAs}(4.2\text{ K})=1.52$ eV from Ref. 28, p. 218, $E_G^{Al_{0.3}Ga_{0.7}As}(4.2\text{ K})=1.8$ eV from Ref. 28, p. 604
m_1^*	$0.0665m_0$	(m_0 is the electron mass), Ref. 28, p. 222, Ref. 72C1
m_2^*	$0.0924m_0$	Ref. 28, p. 334, Ref. 80L1
n_r	3.30	Ref. 28, p. 242, Ref. 62P and 61H
ϵ_1	$12.53\epsilon_0$	(ϵ_0 is the absolute permittivity), Ref. 28, p. 243, Ref. 72R3 and 69J2
ϵ_2	$11.79\epsilon_0$	Ref. 28, p. 167, Ref. 71F (assuming a linear dependence upon GaAs and AlAs for $Al_{0.3}Ga_{0.7}As$)
μ_1	10^5 cm^2/V s	Ref. 28, p. 531 for $T_L=5$ K
μ_2^u	3.8×10^4 cm^2/V s	From Ref. 28, p. 531, Fig. 78, p. 607, Fig. 22 (assuming the same composition dependence of the Hall mobility for 5 and 300 K)
μ_2^d	100 cm^2/V s	Private communication from M. Asche, ZIE, Berlin
N_D^*	1.18×10^{18} cm^{-3}	From Ref. 13 (assuming that the number of ionized carriers is equal to those in the GaAs region)
T_L	5 K	Ref. 13
α	21°	Ref. 15
T	0.5	Ref. 13
L_1	32.5 Å	Ref. 13
L_2^d	50 Å	Ref. 13
L_2^u	200 Å	Ref. 13
τ_{12}	12 ps	Ref. 15
τ_e	0.4 ps	Ref. 27, p. 234
U_0	6 V	(1/1000 of the value in Ref. 8 was assumed)
R_L	283 Ω	Ref. 8
C	1.57×10^{-14} F	Ref. 8
h	3.5×10^{-4} m	Ref. 15
b	10^{-3} m	Ref. 15
l	10^{-2} m	Ref. 15

determined n_2^{u*} must be identified with its definition $n_2^{u(\mathrm{re})}(\Phi_0)$ given in Eqs. (30) and (31). Since E_2 is a linear function of Φ_0 and $n_2^{u(\mathrm{re})}$'s dependence on E_2 yields a resonance behavior via (26), there are zero, one, or two stationary values of Φ_0. It can be shown that there is exactly one for $I=0$ and two for $I>0$.[20]

Due to almost identical $n_1^{(1)*}$, $n_1^{(2)*}$, and n_2^{u*}, the longitudinal current density $j_\parallel^*$ practically coincides for the two resonant steady states. They both show negative differential photoconductivity (NDPC) for IR intensities between a threshold value I_{th} and a saturation intensity I_s as shown in Figs. 4(a) and 4(b) for different lattice temperatures T_L and different effective doping concentrations N_D^*. NPDC is defined here by the negative change of the conductivity $-\Delta\sigma$ with increasing intensity I, normalized by the dark conductivity σ_0 ($I=0$). This explains the negative photoconductivity observed by Heinrich *et al.*,[13] although NDPC was defined there slightly different, viz., with respect to variation of the IR frequency at fixed IR intensity I. Unlike I_s, $I_{\mathrm{th}} \propto \exp(N_D^*/T_L)$ shows a sensitive dependence on the lattice temperature T_L and effective doping concentration N_D^*. Figure 4 shows that the onset of NDPC at low intensities is favored by low lattice temperatures and high doping concentrations, as indeed applied in Ref. 13. It is not sensitive to a variation of the GaAs QW width $2L_1=65-90$ Å.

In the nonresonant regime, the photoconductivity of the only existing steady state $\mathbf{x}^{*(\mathrm{nr})}$ remains practically constant at the dark value σ_0 for all IR intensities, since the absolute value of the nonresonant-tunneling currents there is too small to permit a measurable number of carriers to leave the GaAs QW and enter the $Al_xGa_{1-x}As$ region. Additionally, considering diffusion currents across the interface would reduce $\sigma^{*(\mathrm{nr})}$ to $\sigma^{*(\mathrm{nr})}<\sigma_0$, but would not influence the practically vanishing negative photoconductivity of the nonresonant steady state, since diffusion does not distinguish between the ground and the excited GaAs subband.

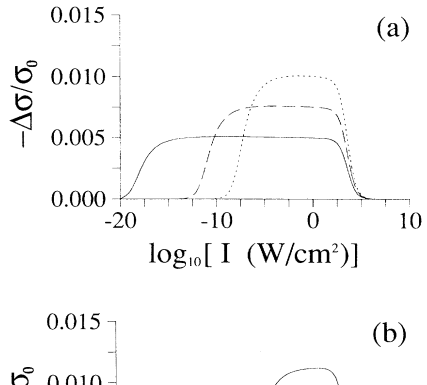

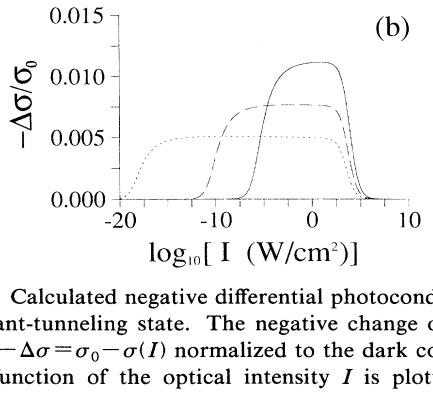

FIG. 4. Calculated negative differential photoconductivity of the resonant-tunneling state. The negative change of the conductivity $-\Delta\sigma=\sigma_0-\sigma(I)$ normalized to the dark conductivity σ_0 as a function of the optical intensity I is plotted (a) for different lattice temperatures $T_L=5$ K (solid line), $T_L=7.5$ K (dashed line), and $T_L=10$ K (dotted line), and (b) for different effective doping concentrations $N_D^*=5.0\times10^{17}$ cm^{-3} (solid line), $N_D^*=7.5\times10^{17}$ cm^{-3} (dashed line), and $N_D^*=1.18\times10^{17}$ cm^{-3} (dotted line). (Parameters cf. Table I.)

The stability of the steady states $\mathbf{x}^{*(\mathrm{ri})}$, $i=1,2$, and $\mathbf{x}^{*(\mathrm{nr})}$ against infinitesimal fluctuations $\delta\mathbf{x}(t)=\delta\mathbf{x}(0)\exp(\lambda t)$ is determined by linearizing the dynamical system around each steady state and computing the eigenvalues λ of the Jacobian matrix $J(\mathbf{x}^*)_{ij}=(\partial\dot{x}_i/\partial x_j)^*$, $i,j=1,\ldots,5$. We find that the incident radiation leads to a supercritical pitchfork bifurcation, since $\mathbf{x}^*$, which is a stable node (e.g., all eigenvalues negative) at $I=0$, splits up into the two stable nodes $\mathbf{x}^{*(r2)}$ and $\mathbf{x}^{*(\mathrm{nr})}$, and the saddle $\mathbf{x}^{*(r1)}$ (1 positive, 4 negative eigenvalues) for $I>0$, where the eigenvector corresponding to $\mathbf{x}^{*(r1)}$'s unstable mode coincides with the Φ_0 coordinate axis in the system's phase space $(n_1^{(1)}, n_1^{(2)}, \varepsilon_\parallel, \Phi_0, \Phi_1)^T$.

Each fixed point possesses one (negative) eigenvalue, the order of magnitude of whose absolute value can be tuned with the IR intensity. Thus, unlike the typical time scale of the interlayer transitions and the transversal dielectric relaxation in $Al_xGa_{1-x}As$, the time scale on which carrier exchange between the two GaAs subbands occurs varies with I.

The linear bifurcation analysis therefore shows that under IR excitation ($I>0$) bistability between the two stable steady states $\mathbf{x}^{*(r2)}$ and $\mathbf{x}^{*(\mathrm{nr})}$ occurs (Fig. 3). This optoelectronic bistability can be illustrated by a reinterpretation of Fig. 3 in terms of stable resonant and nonresonant tunneling states. The solid line corresponds to the I-independent nonresonant states $\mathbf{x}^{*(\mathrm{nr})}$, while the dashed and dotted lines, depending on I, correspond to the stable resonant state $\mathbf{x}^{*(r2)}$. It should be noted that self-generated oscillatory instabilities as found for electrically induced real-space transfer[7-10] do not occur for any optical intensity.

V. RESULTS AND DISCUSSION

The linear bifurcation analysis implies that the dynamical system given by Eqs. (5), (7), (17), (18), and (20) shows *optoelectronic bistability*, which is confirmed by numerical time-dependent simulations of this system.[20] A differentiable connex manifold containing $\mathbf{x}^{*(r1)}$ separates the phase space into two attractor basins for the resonant and nonresonant stable nodes $\mathbf{x}^{*(r2)}$ and $\mathbf{x}^{*(\mathrm{nr})}$, respectively. In the nonresonant-tunneling state $\mathbf{x}^{*(\mathrm{nr})}$ practically all carriers reside in the GaAs QW, the conductivity is high, and Φ_0 is small, whereas in the resonant tunneling states $\mathbf{x}^{*(r2)}$ the carriers are increasingly real-space transferred to the $Al_xGa_{1-x}As$ barrier with increasing IR intensity, the conductivity decreases and Φ_0 is large (Fig. 5). Which state actually will be realized depends

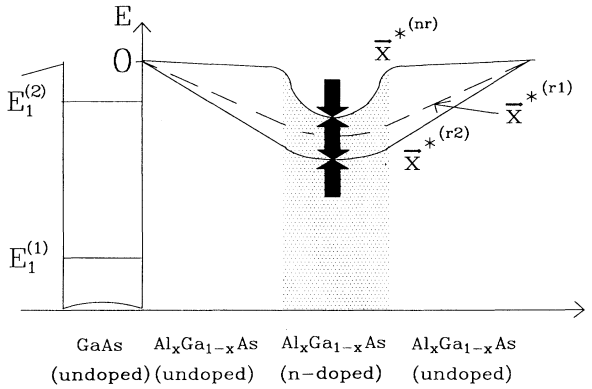

FIG. 5. Band structure corresponding to the three steady states (schematic). The middle state $\mathbf{x}^{*(r1)}$ is unstable and lies within the separatrix manifold separating the attractor basins of the stable steady states $\mathbf{x}^{*(r2)}$ (resonant) and $\mathbf{x}^{*(nr)}$ (nonresonant tunneling).

upon the initial conditions chosen. We propose to consider this effect for application as a *picosecond optoelectronic switch.* Figure 6 shows that a small fluctuation in the potential barrier height Φ_0 causing it to drop below the value at $\mathbf{x}^{*(r1)}$ leads to a transition from the low conductivity ($\mathbf{x}^{*(r2)}$) to the high conductivity steady state ($\mathbf{x}^{*(nr)}$) in less than 5 ps.

The bistability as displayed by the above system is not a feature restricted to the explicit form of its equations, but holds on very few generalized conditions. This is

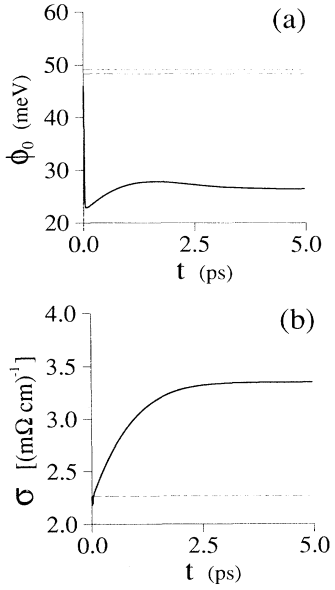

FIG. 6. Calculated temporal evolution (a) of the barrier height Φ_0 and (b) of the conductivity σ after a small fluctuation forces Φ_0 to become smaller than the value corresponding to $\mathbf{x}^{*(r2)}$ [lower dashed-dotted line in (a)]. The system switches from the low conductivity resonant steady state [dashed-dotted line in (b)] to the high conductivity nonresonant steady state in less than 5 ps. ($I = 1.0 \times 10^6$ W/cm^2, other parameters cf. Table I.)

shown in the Appendix. We therefore conclude that it is generic for optically induced real-space transfer in modulation-doped GaAs/$Al_xGa_{1-x}As$ heterostructures with two relevant subbands in the GaAs QW. The different differential photoconductivities displayed in the two locally stable regimes, on the other hand, can only be explained by the explicit model equations, where the resonant and nonresonant tunneling currents have been considered quantitatively. Our model provides a detailed theory to the NDPC measured by Heinrich *et al.*[13] and optoelectronic bistability as found by Zrenner.[26]

VI. CONCLUSIONS

We have shown that real-space transfer can be induced in a modulation-doped semiconductor heterostructure by intersubband excitation of electrons in the GaAs quantum well due to infrared absorption and subsequent tunneling. A system of nonlinear dynamic model equations has been derived, incorporating the 2D generation-recombination kinetics in GaAs, the space-charge dynamics of the $Al_xGa_{1-x}As$ barrier, resonant and nonresonant tunneling across the GaAs/$Al_xGa_{1-x}As$ interface, and dielectric relaxation of the parallel electric field. The steady states, their stability, and the transient behavior have been analyzed with the methods of nonlinear dynamics. We predict optoelectronic bistability associated with different photoconductive responses of the two stable steady states: the state of dominant resonant tunneling currents shows negative IR photoconductivity, whereas the nonresonant tunneling state is practically independent of the IR intensity. Ultrafast switching behavior between these two steady states is suggested for potential applications.

ACKNOWLEDGMENTS

We are indebted to R. Döttling, M. Asche, and D. Reznik for elucidating discussions.

APPENDIX: GENERAL CONDITIONS FOR BISTABILITY

In the following we consider a generalized model system for the dynamic variables $n_1^{(1)}$, $n_1^{(2)}$, Φ_0, and Φ_1 independent of the assumption of a specific model. (For small U_0, $\varepsilon_\parallel$ can be assumed to have no influence on the other variables.) The set of differential equations governing the variable's temporal behavior is assumed to meet the following conditions:

(i) $\dot{n}_1^{(1)}$ and $\dot{n}_1^{(2)}$ are given by Eqs. (5) and (7), respectively, where $j_\perp$ in (7) is substituted by the generalized current density $\tilde{j} \equiv \tilde{j}^{re} + \tilde{j}^{(nr)}$. $\tilde{j}^{(re)}$ and $\tilde{j}^{(nr)}$ may be arbitrary twice continuously differentiable functions of the dynamic variables with the restriction that $\tilde{j}^{(re)}$'s dependence upon Φ_0 has the form of a resonance curve, $\tilde{j}^{(nr)}$ is a monotonically decreasing function of Φ_0, and both $\tilde{j}^{(re)}$ and $\tilde{j}^{(nr)}$ are proportional to $-n_1^{(2)}$ and n_2 near the system's fixed points. Additionally $\tilde{j}$'s dependence on Φ_1 is assumed to be small.

(ii) Φ_1's time dependence is governed by

$\dot{\Phi}_1 = f(n_1^{(1)}, n_1^{(2)}) - \Phi_1$ with $f > 0$ for all $n_1^{(1)}$ and $n_1^{(2)}$.

(iii) $n_2^u(n_1^{(1)}, n_1^{(2)}, \Phi_0, \Phi_1)$ results exclusively from carrier transport through the undoped $Al_xGa_{1-x}As$ region.

(iv) Near each fixed point $d(\Phi_0 - \Phi_1)/dt$ increases monotonically as a function of n_2^u.

(v) Φ_0 is a fast variable.

The first two restrictions in (i) reflect the E_2 dependence the tunneling currents have due to their physical features. They hold since E_2 must be a monotonic function of Φ_0. The third one is a minimum prerequisite physically reasonable currents must meet. The fourth reflects the fact that E_2 depends much more on the potential height Φ_0 than on the potential form condition. (ii) results from Eq. (12), taking into account $n_2^u \ll n_1^{(1)}$, $n_1^{(2)}$. Condition (iv) is assumed since an increase of the carrier density in the undoped region leads to a stronger curvature of $\Phi(x)$ there, increasing $\Phi_0 - \Phi_1 \equiv \Phi(L_2^u) - \Phi(0)$. Condition (v) holds if the dielectric relaxation time $\tau_M \equiv \epsilon_2/(e\mu_2^d N_D^*)$ is small due to a high doping concentration.

Taking into account carrier conservation, the third condition in (i) leads to

$$\delta\tilde{j}^{(\mathrm{re/nr})} = c - b^{(\mathrm{re/nr})}(\Phi_0, \Phi_1) n_1^{(1)} - (a^{(\mathrm{re/nr})} + b^{(\mathrm{re/nr})})(\Phi_0, \Phi_1) n_1^{(2)} , \tag{A1}$$

where $a^{(\mathrm{re/nr})}, b^{(\mathrm{re/nr})} > 0$, $c = L_2^d/L_2$ holds, for small deviations $\delta\tilde{j}^{(\mathrm{re/nr})}$, from the steady-state value $\tilde{j}^* \equiv 0$.

Computation of the Jacobi matrix J for the $(n_1^{(2)}, n_1^{(1)})$ subsystem at any fixed point $\mathbf{x}^*$ leads to

$$J = \begin{pmatrix} J_{11} & J_{12} \\ -J_{11} - b & -J_{12} - (a+b) \end{pmatrix} , \tag{A2}$$

with $J_{1i} = \partial \dot{n}_1^{(1)}/\partial n_1^{(i)}(\mathbf{x}^*), i = 1,2$. For J_{11} and J_{12},

$$J_{11} \propto \xi_1 \frac{\xi_2 - 1}{(\xi_2 - \xi_1)^2}(n_1^{(2)} - n_1^{(1)})(\mathbf{x}) < 0 ,$$
$$J_{12} \propto \xi_2 \frac{\xi_1 - 1}{(\xi_2 - \xi_1)^2}(n_1^{(1)} - n_1^{(2)})(\mathbf{x}) > 0 , \tag{A3}$$

hold, where $\xi_i \equiv \exp(n_i^{(i)}/n_{c_1})$, $i = 1,2$ was introduced for convenience. The signs of J_{11} and J_{12} are always valid, since occupation inversion $n_1^{(2)^*} > n_1^{(1)^*}$ in the steady state is impossible in this two-subband model. Computation of the trace T and determinant D results in

$$T = J_{11} - J_{12} - (a+b) < 0 , \tag{A4}$$

$$D = bJ_{12} - (a+b)J_{11} > 0 . \tag{A5}$$

Thus all the system's fixed points are stable against fluctuations in the $(n_1^{(1)}, n_1^{(2)})$ plane. Condition (iii) and the last condition in (i) then assures stability in the Φ_1 direction as well, if Φ_0 can be eliminated adiabatically [which is the case due to (v)].

For a stability analysis of fluctuations of Φ_0, the resonant and nonresonant regime must be distinguished: in the steady state where $\tilde{j}^{(\mathrm{nr})^*} \gg \tilde{j}^{(\mathrm{re})^*}$ holds, the fixed point $\mathbf{x}^{*(\mathrm{nr})}$ is stable, since due to (iv) and the second condition in (i) a fluctuation $\delta\Phi_0$, e.g., $\delta\Phi_0 > 0$, implies a decrease of n_2^u, and due to (iv), of $\Phi_0 - \Phi_1$. Since Φ_1 can be considered independent of n_2^u because of (iii), Φ_0 relaxes back to its steady-state value. Analogous relaxation occurs for $\delta\Phi_0 < 0$. In the case of $\tilde{j}^{(\mathrm{re})} \gg \tilde{j}^{(\mathrm{nr})}$ we obtain two steady states $\Phi_0^{*(r1)}$ and $\Phi_0^{*(r2)}$ with $\Phi_0^{*(r1)} < \Phi_0^{*(r2)}$ due to the first condition for $\tilde{j}$ in (i), where the values lie on either side of the resonance curve maximum. Thus n_2^u is a decreasing function of Φ_0 at $\Phi_0^{*(r2)}$ and $\mathbf{x}^{*(r2)}$ is stable against fluctuations of Φ_0 by the same argument as for $\mathbf{x}^{*(\mathrm{nr})}$. $\mathbf{x}^{*(r1)}$, on the other hand, is unstable since n_2^u rises with Φ_0 at $\Phi_0^{*(r1)}$.

Therefore, the local conditions in (i)–(iv) together with (v) generate two stable nodes and a saddle as fixed points. If the dynamic system has unique solutions and the physical phase space is bounded, these conditions are sufficient for the system to display a bistable behavior.

*Present address: Department of Chemistry, The University of Chicago, 5735 South Ellis Avenue, Chicago, IL 60637.

[1]K. Hess and G. J. Iafrate, in *Heterojunction Band Discontinuities,* edited by F. Capasso and G. Margaritondo (North-Holland, Amsterdam, 1987).

[2]*Negative Differential Resistance and Instabilities in 2-dimensional Semiconductors,* edited by N. Balkan, B. K. Ridley, and A. J. Vickers (Plenum, New York, 1993).

[3]Z. S. Gribnikov, Fiz. Tekh. Poluprovodn. **6**, 1380 (1972) [Sov. Phys. Semicond. **6**, 1204 (1973)].

[4]F. Pacha and F. Paschke, Electron. Commun. **32**, 235 (1978).

[5]K. Hess, H. Morkoc, H. Shichijo, and B. G. Streetman, Appl. Phys. Lett. **35**, 469 (1979).

[6]P. D. Coleman, J. Freeman, H. Morkoc, K. Hess, B. G. Streetman, and M. Keever, Appl. Phys. Lett. **40**, 493 (1982).

[7]E. Schöll and K. Aoki, Appl. Phys. Lett. **58**, 1277 (1991).

[8]K. Aoki, K. Yamamoto, N. Mugibayashi, and E. Schöll, Solid State Electron. **32**, 1149 (1989).

[9]E. Schöll and K. Aoki, in *Proceedings of the Twentieth International Conference on the Physics of Semiconductors,* edited by E. H. Anastassakis and J. D. Joannopoulos (World Scientific, Singapore, 1990), p. 1125.

[10]R. Döttling and E. Schöll, Phys. Rev. B **45**, 1935 (1992).

[11]L. C. West and S. J. Eglash, Appl. Phys. Lett. **46**, 1146 (1985).

[12]B. F. Levine, R. J. Malik, J. Walker, K. K. Choi, C. G. Bethea, D. A. Kleinman, and J. M. Vandenburg, Appl. Phys. Lett. **50**, 273 (1987).

[13]R. Heinrich, R. Zachai, M. Besson, T. Egeler, G. Abstreiter, W. Schlapp, and G. Weimann, Surf. Sci. **228**, 465 (1990).

[14]S. Luryi, Appl. Phys. Lett. **58**, 1727 (1991).

[15]A. Seilmeier, H. J. Hübner, G. Abstreiter, G. Weimann, and W. Schlapp, Phys. Rev. Lett. **59**, 1345 (1987).

[16]E. Schöll, Solid State Electron. **32**, 1129 (1989).
[17]M. J. Adams and P. T. Landsberg, in *Gallium Arsenide Lasers,* edited by C. H. Gooch (Wiley, London, 1969).
[18]J. A. Levenson, G. Doloque, J. L. Oudau, and I. Abram, Solid State Electron. **32**, 1869 (1989).
[19]J. Shah, Solid State Electron. **32**, 1051 (1989).
[20]R. E. Kunz, diploma thesis, Technical University of Berlin, 1992.
[21]E. E. Mendez, in *Applications of Quantum Wells and Superlattices,* Vol. 170 of *NATO Advanced Study Institute,* edited by E. E. Mendez and K. v. Klitzing (Plenum, New York, 1987).
[22]S. Luryi, Superlatt. Microstruct. **5**, 375 (1989).
[23]L. D. Landau and E. M. Lifschitz, *Lehrbuch der theoretischen Physik* (Akademie, Berlin, 1979), Vol. 3.
[24]D. N. Poenaru and M. S. Irascu, in *Particle Emission from Nuclei,* edited by D. N. Poenaru and M. S. Irascu (CRC, Boca Raton, 1989).
[25]M. Büttiker and R. Landauer, Phys. Rev. Lett. **49**, 1742 (1982).
[26]A. Zrenner, in *Festkörperprobleme (Advances in Solid State Physics),* edited by U. Rössler (Vieweg, Braunschweig, 1992), Vol. 32.
[27]K. Hess and G. J. Iafrate, in *Hot Electron Transport in Semiconductors,* edited by L. Reggiani (Springer, Berlin, New York, 1985).
[28]*Physics of Group IV Elements and III-V Compounds,* edited by O. Madelung, Landolt-Börnstein, New Series, Group 17, Vol. III, Pt. a (Springer, Berlin, 1982).